Electronic Supplementary Material (ESI) for Physical Chemistry Chemical Physics.

Supplementary Information

Enhanced intramolecular charge transfer and near-infrared fluorescence in 4-dimethylamino-chalcone analogues through extended conjugation: synthesis, photophysical properties, and theoretical modelling

Balqees S. Al-Saadi, A. Ramadan Ibrahim, John Husband,* Ahmed H. Ismail, Younis Baqi,* and Osama K. Abou-Zied*

Department of Chemistry, College of Science, Sultan Qaboos University, P.O. Box 36, Postal Code 123, Muscat, Sultanate of Oman

* Corresponding Authors: johnh@squ.edu.om (JH); baqi@squ.edu.om (YB); abouzied@squ.edu.om (OKA-Z)

Femtosecond pump-probe transient absorption setup

The ultrafast transient absorption measurements were performed using a femtosecond laser setup that was previously described in detail.[1,2] Briefly, pump and probe pulses were obtained using a regenerative amplified Ti:Sapphire laser (Libra, Coherent). The Libra generates compressed laser pulses (70 fs pulse width) with an output power of 4.26 W at a repetition rate of 5 kHz and centered at 800 nm. The output beam was split into two parts. The major portion of the output pulse was used to pump a Coherent OPerA Solo (Light Conversion Ltd.) optical parametric amplifier to generate spectrally tunable light spanning the range 240−2600 nm and is used as the pump beam. The remaining small portion of the laser output was focused on a sapphire crystal to generate a white light continuum in the range 420-800 nm which is used as the probe beam in a Helios transient absorption spectrometer (Ultrafast Systems, LLC). The probe light was measured by a fiber optic that is coupled to a multichannel spectrometer with a CMOS sensor in the range 350-850 nm. Chirp in the white light continuum probe was minimized by using parabolic mirrors. Rotational contribution to the overall excited state decay kinetics was removed by depolarizing the pump beam using a depolarizer (DPU-25, Thorlabs). The pump pulse was attenuated to ~100 nJ in order to avoid multiphoton excitation.

The pump and probe pulses were focused on the sample and the temporal delay of the probe pulse was varied using a computer-controlled optical delay stage. Kinetic traces at appropriate wavelengths were assembled from the time-resolved spectral data. Surface Xplorer software (supplied by Ultrafast Systems) was used for data analysis. In order to adjust the zero delay for each wavelength and to get the chirp-corrected spectrum, we carried out the transformation process using the software program (Surface Xplore). The instrument response function (IRF) was measured from Raman scattering to be ~ 120 fs.

Femtosecond fluorescence-upconversion setup

A Halcyone fluorescence upconversion setup (Ultrafast Systems, LLC) was used to measure the femtosecond fluorescence dynamics. The femtosecond laser system, employed in the transient absorption setup, was used by removing two movable mirrors in order to direct the pump and probe (gate) beams to the Halcyone box. The gate pulse was delayed with a computer-controlled optical delay stage. The pump pulse was focused onto the sample and fluorescence was collected and focused by a parabolic mirror on a 0.5 mm BBO type II crystal. For frequency upconversion, the gate pulse (800 nm) was overlapped with the fluorescence signal in the BBO crystal, and focused slightly behind the crystal (~ 10 mm). The upconversion signal was focused on the entrance slit of a double monochromator and measured by a PMT detector with a spectral range of 200−800 nm. A depolarizer (DPU-25, Thorlabs) was used in the pump beam (attenuated to < 100 nJ) in order to remove any rotational contribution to the overall excited state decay kinetics. The IRF under the current non-collinear geometry was determined to be 400–500 fs from the upconversion signal of Raman scattering from water. Surface Xplorer software was used for data analysis.

The samples in solution for the lifetime measurements were prepared in 2 mm fused silica cuvettes (Spectrocell Inc.) and were stirred during the experiment. All measurements were conducted at 22.0 ± 0.5 °C.

NMR spectra for 2DHC, 2DC, 3DHC, and 3DC

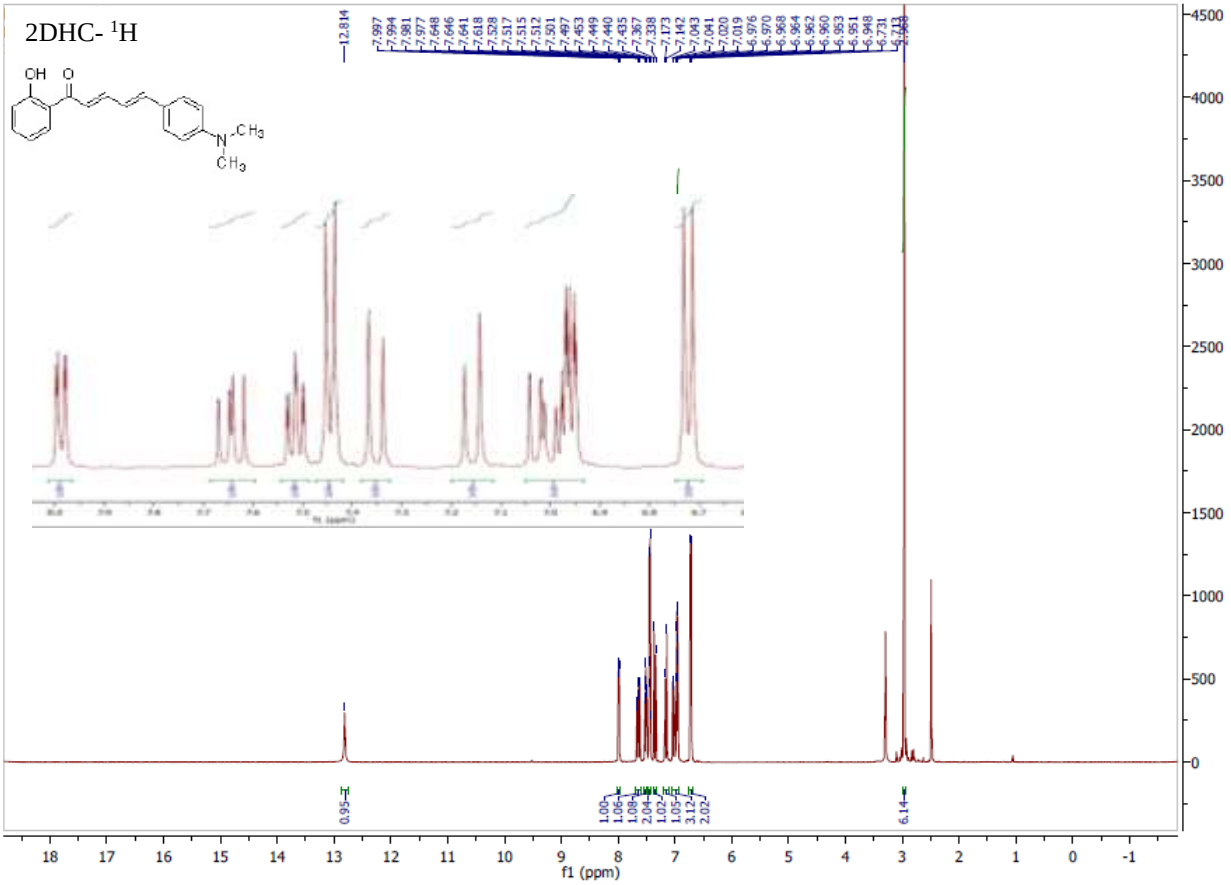

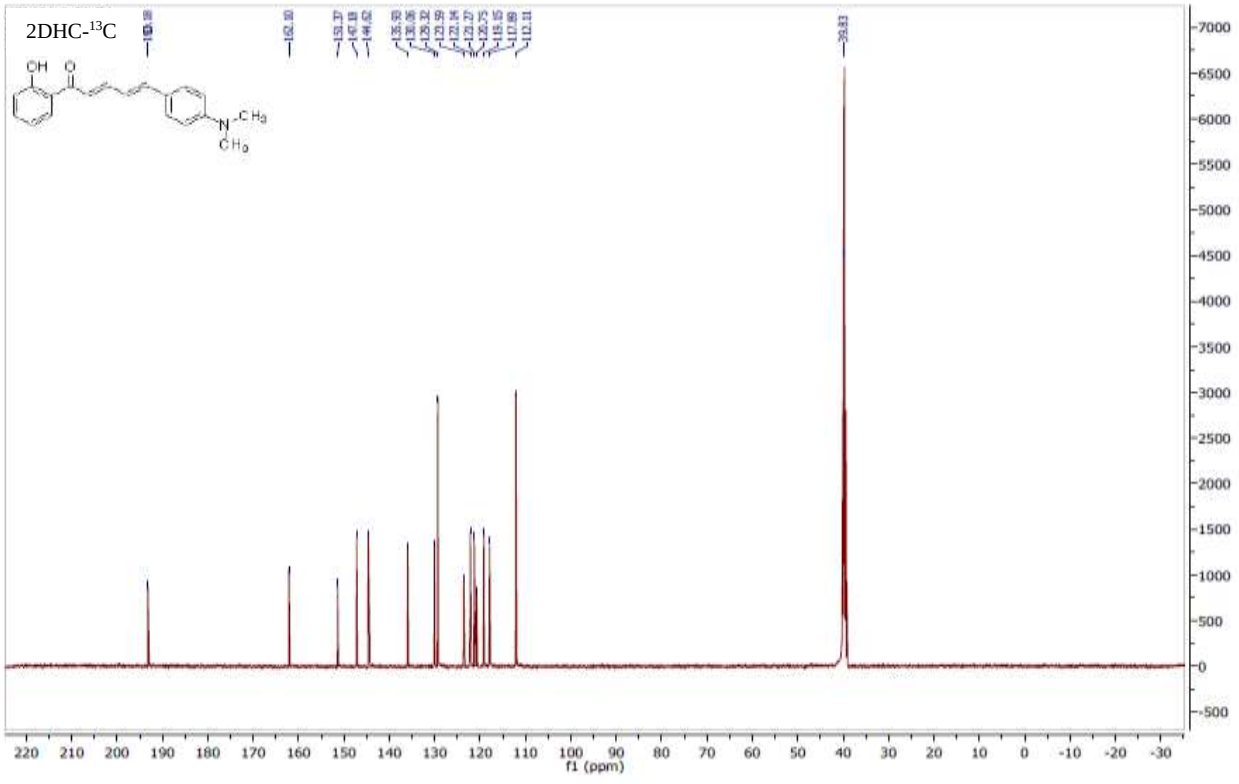

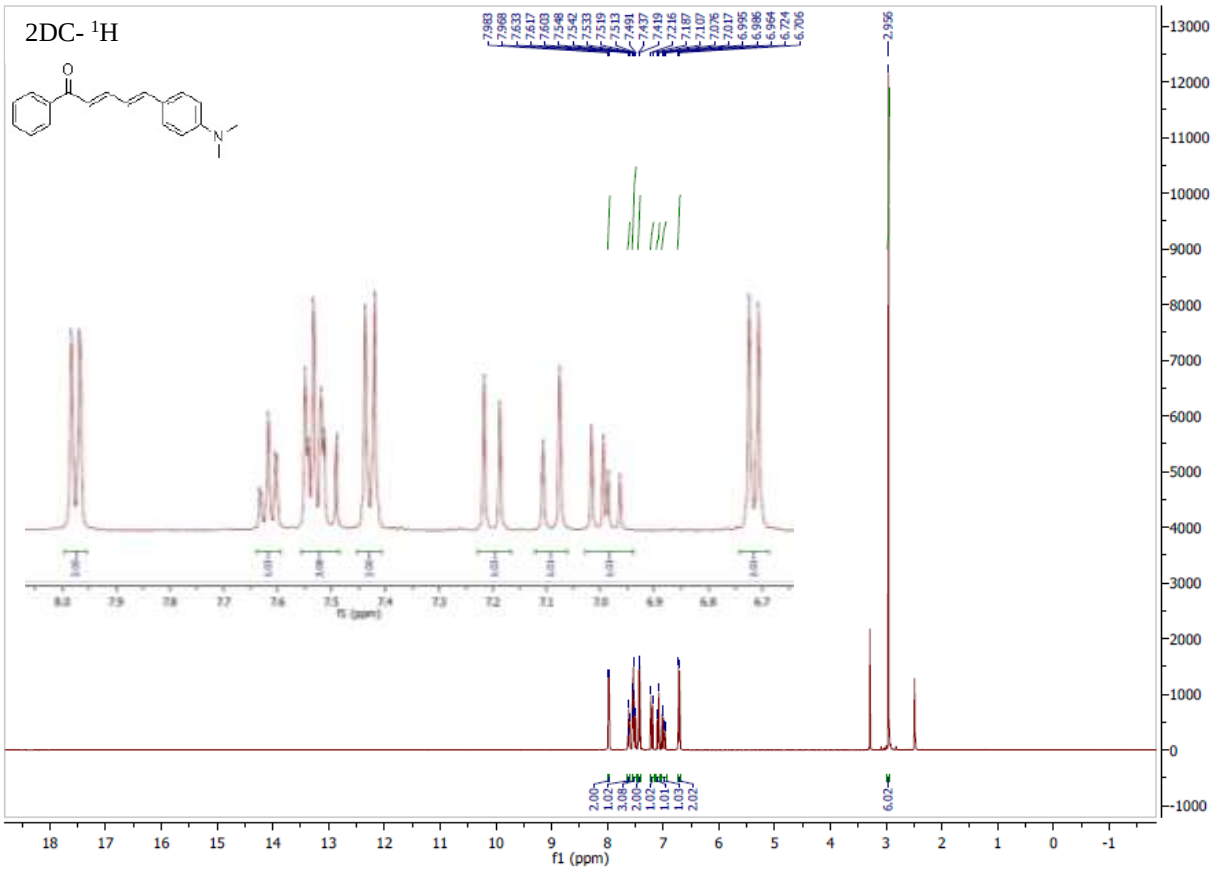
2DC- 1H
f1 (ppm)

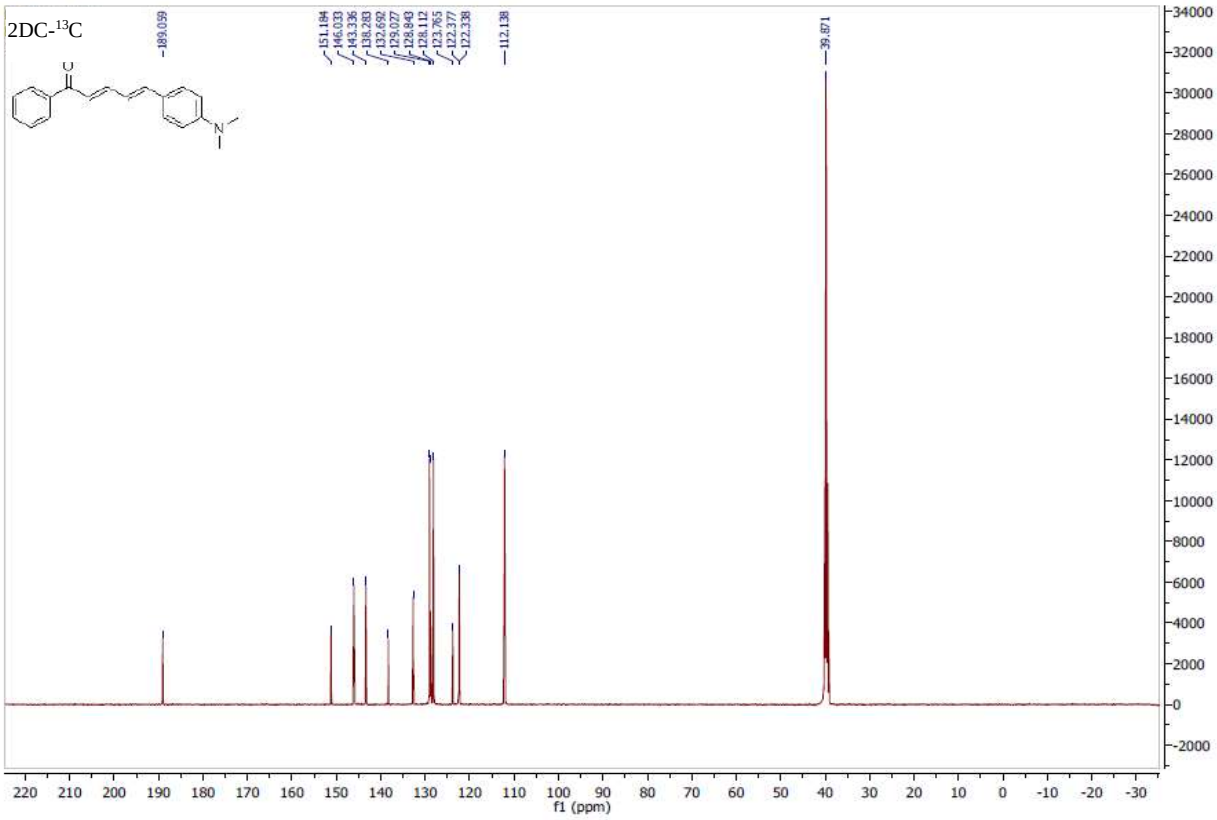
2DC-13C
f1 (ppm)

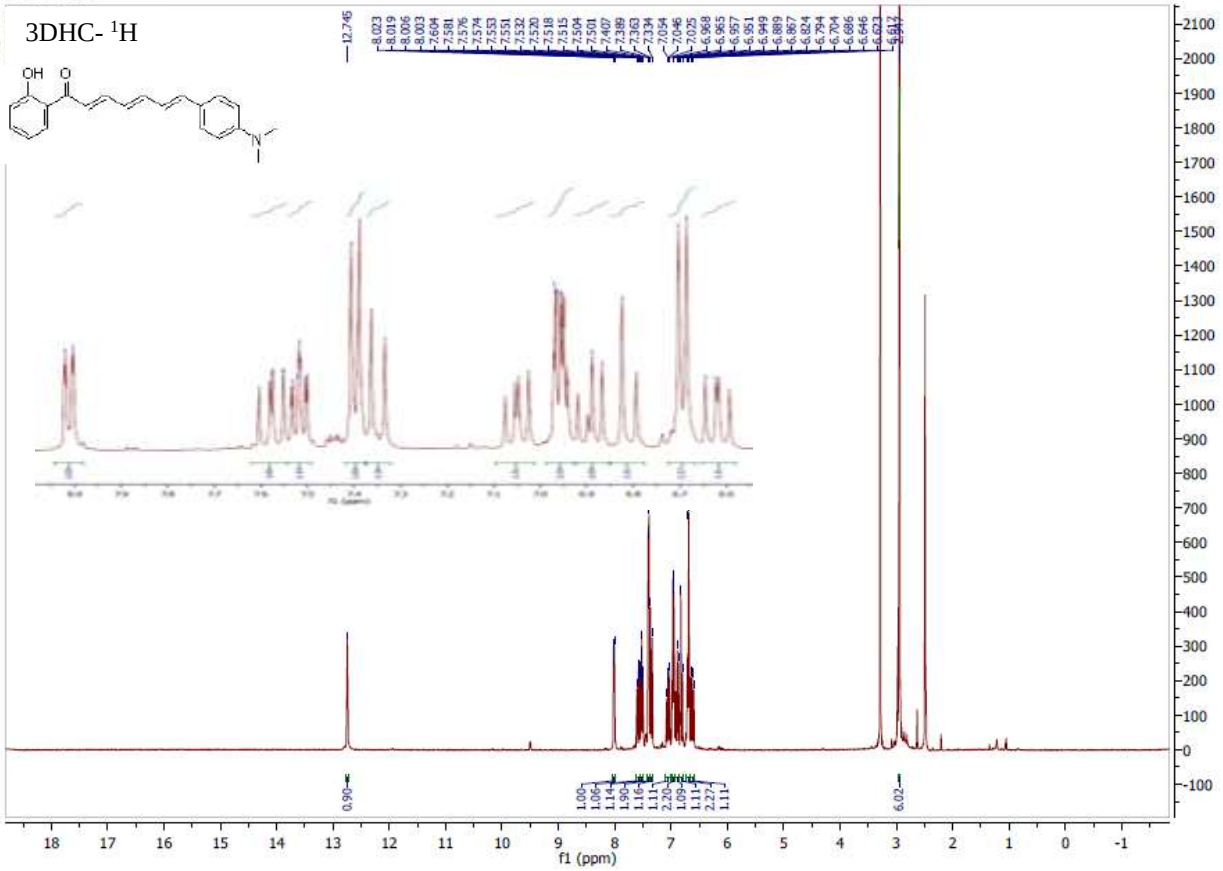
3DHC- 1H
OH
O
N
f1 (ppm)

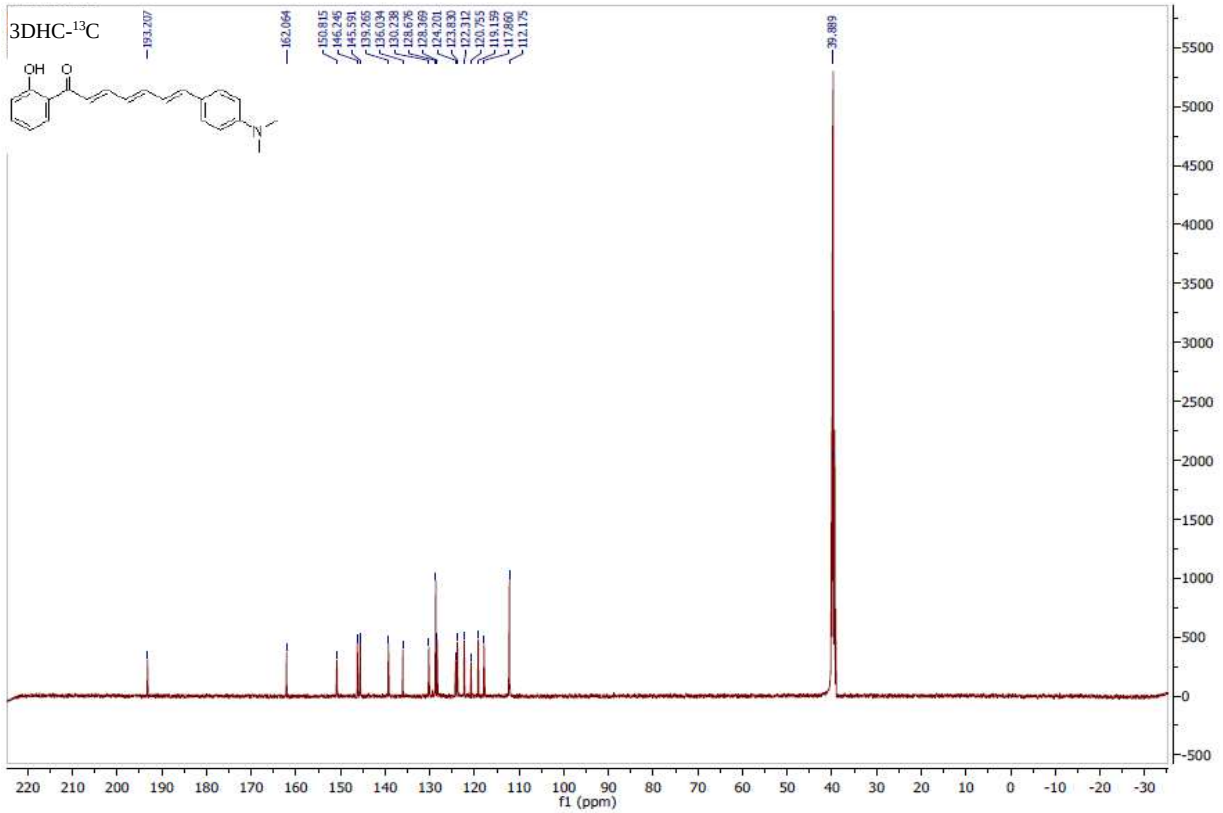
3DHC-13C
OH
O
N
f1 (ppm)

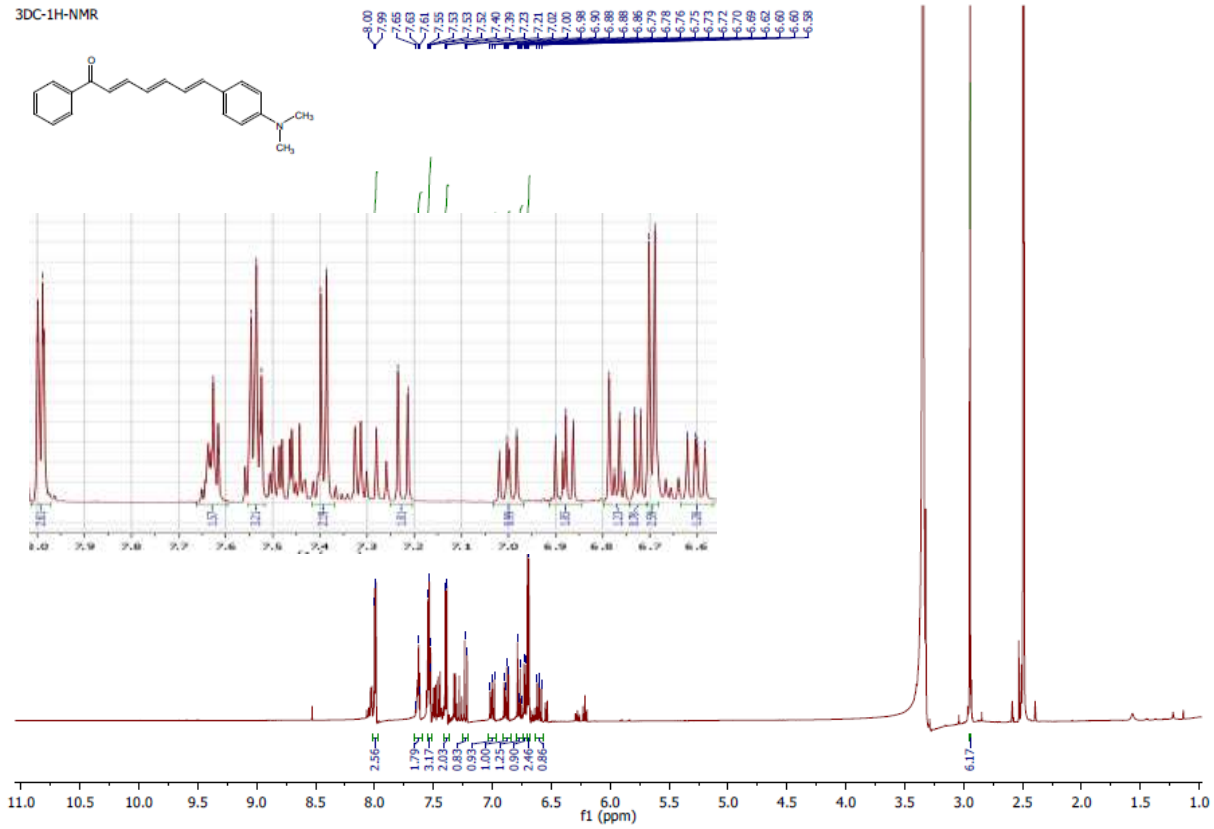
3DC-1H-NMR
f1 (ppm)

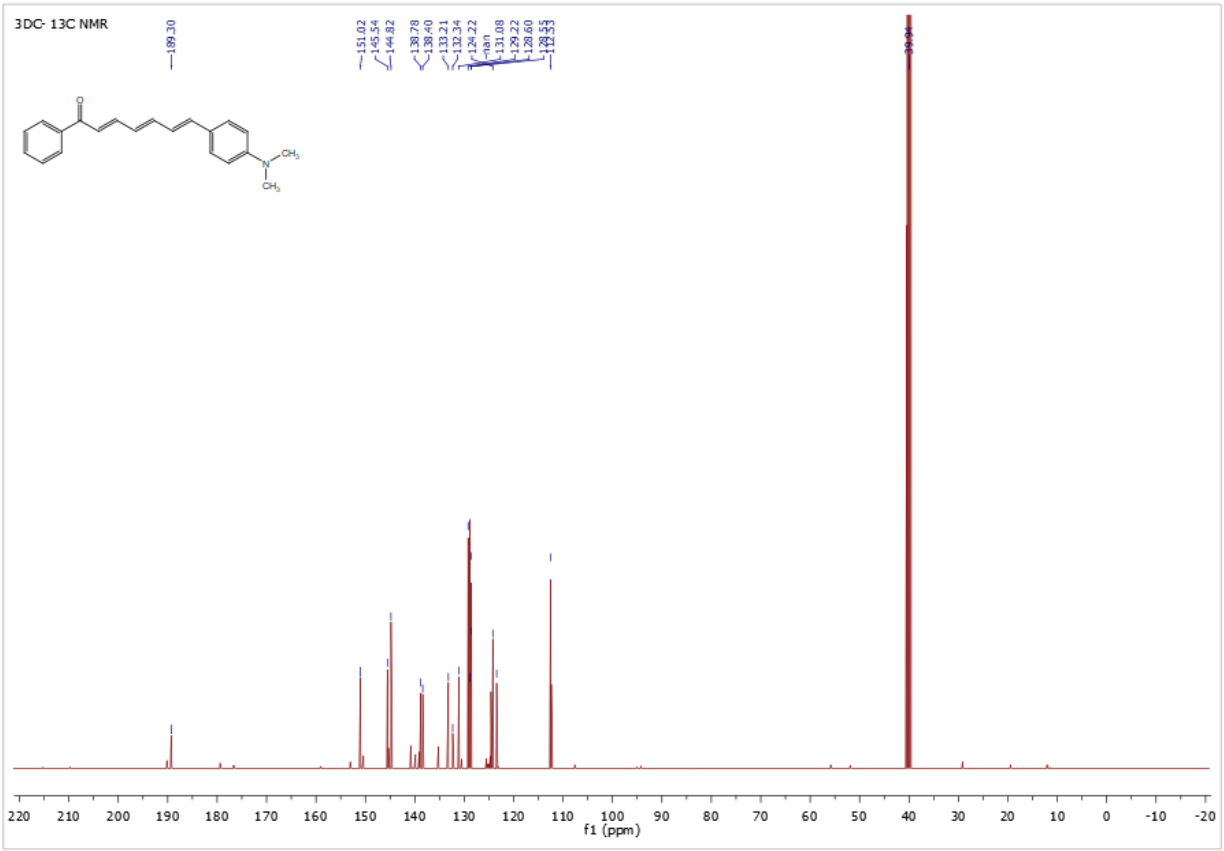
3DC- 13C NMR
f1 (ppm)

Table S1 FWHM of absorption and fluorescence spectra (nm).

DHC	2DHC	3DHC	DC	2DC	3DC
Absorption					
76	98	111	79	96	109
Fluorescence					
107	107	135	103	103	134

Fluorescence decay transients

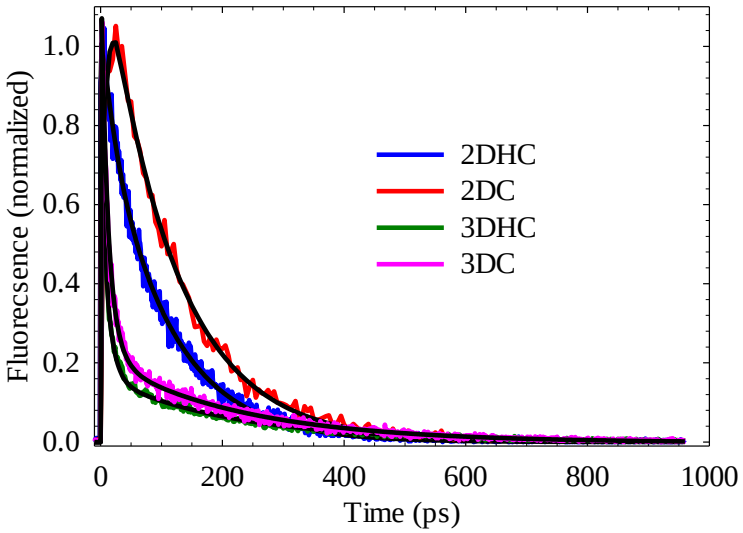

Fig. S1 Fluorescence decay transients for the chalcone derivatives dissolved in MeOH, measured by fluorescence upconversion. Solid line represents the best fit to a multi-exponential decay function. IRF = 450 fs, λ_{ex} = 450 nm, and $\lambda_{detection}$ = 700 nm.

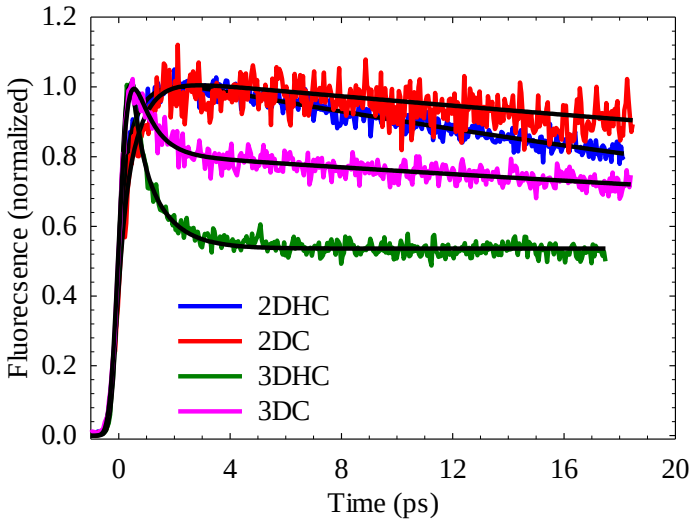

Fig. S2 Fluorescence decay transients for the chalcone derivatives dissolved in acetonitrile, measured by fluorescence upconversion. Solid line represents the best fit to a multi-exponential decay function. IRF = 450 fs, λ_{ex} = 450 nm, and $\lambda_{detection}$ = 700 nm.

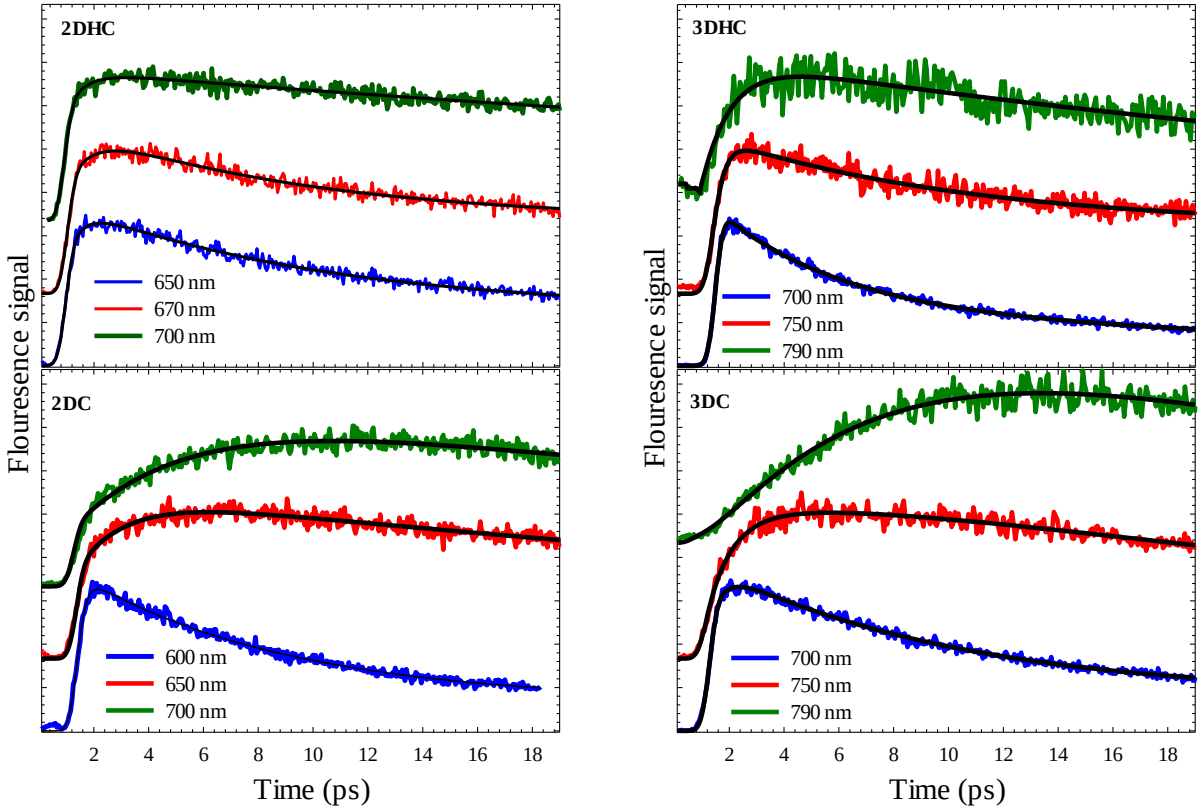

Fig. S3 Fluorescence decay transients for the chalcone derivatives dissolved in MeOH, measured by fluorescence upconversion at three different detection wavelengths, as shown in each graph. IRF = 450 fs, λ_{ex} = 450 nm.

Transient absorption dynamics

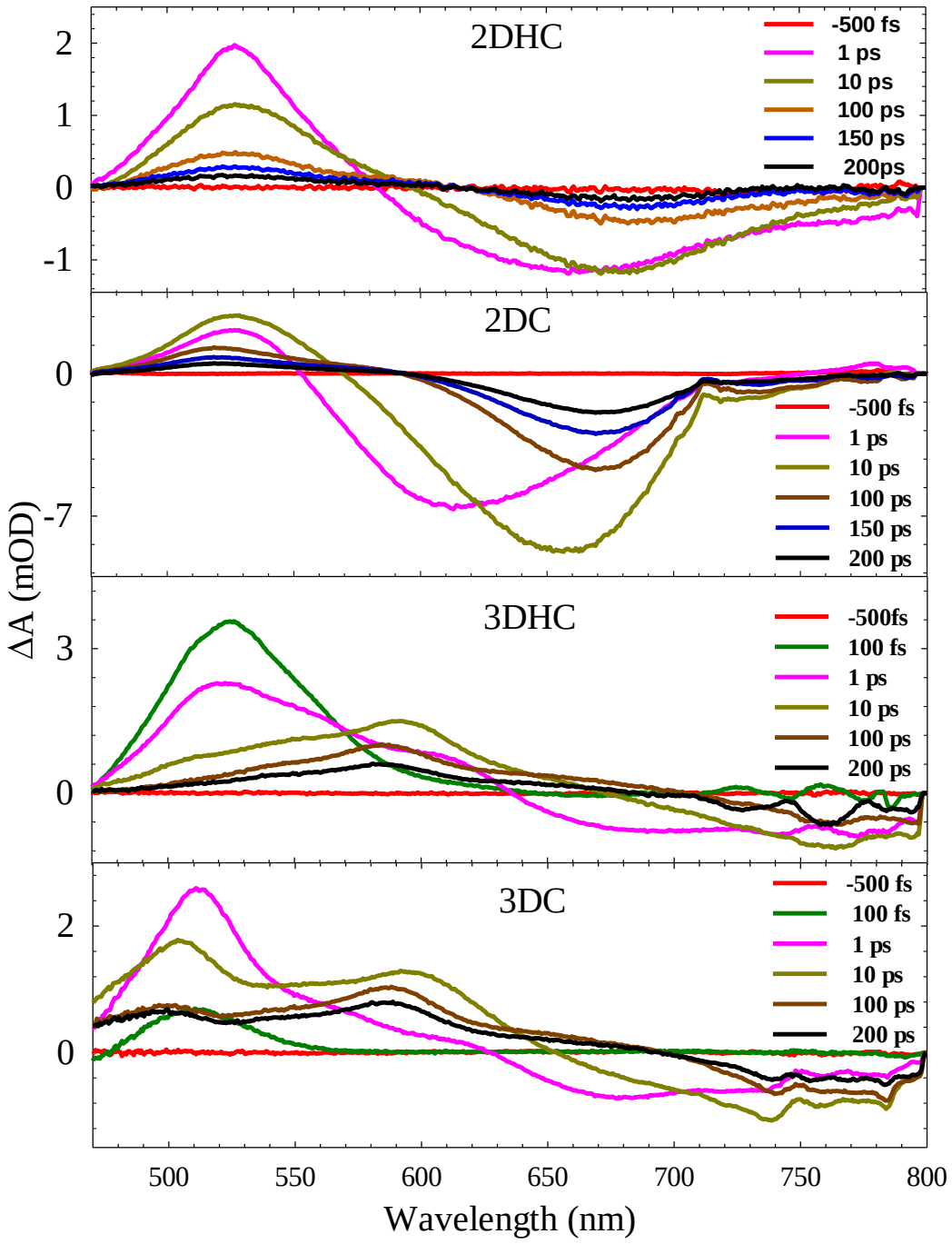

Fig. S4 Transient absorption spectra of the chalcone derivatives dissolved in MeOH. λ_{ex} = 450 nm.

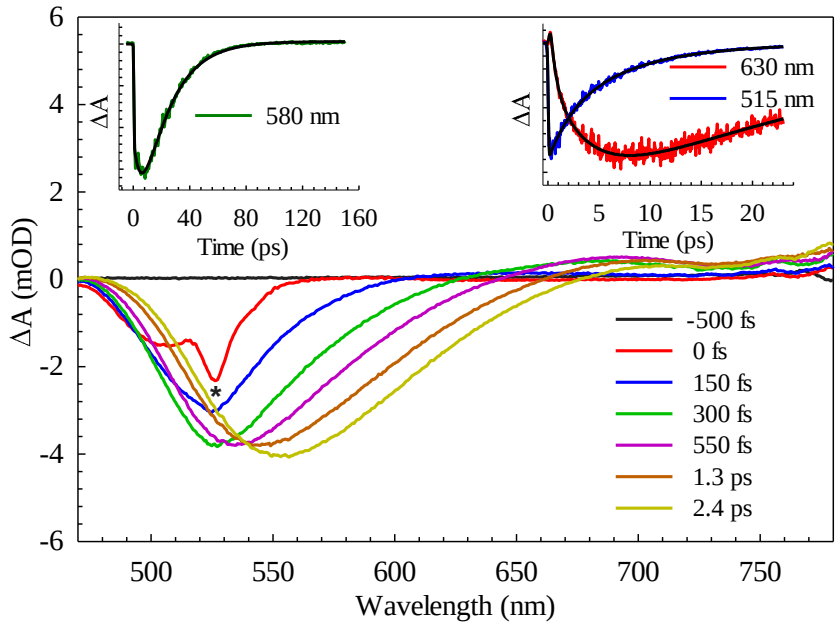

Fig. S5 Transient absorption spectra of DC dissolved in MeOH. The right inset displays solvent dynamics with a rise in the red-side and decay on the blue side. Meanwhile, the left inset exhibits the entire time decay range (refer to Table 2 in the paper for specific time constants). The distorted band at 0 fs delay time (*) illustrates the emergence of Raman scattering due to solvent. IRF = 120 fs, λ_{ex} = 450 nm.

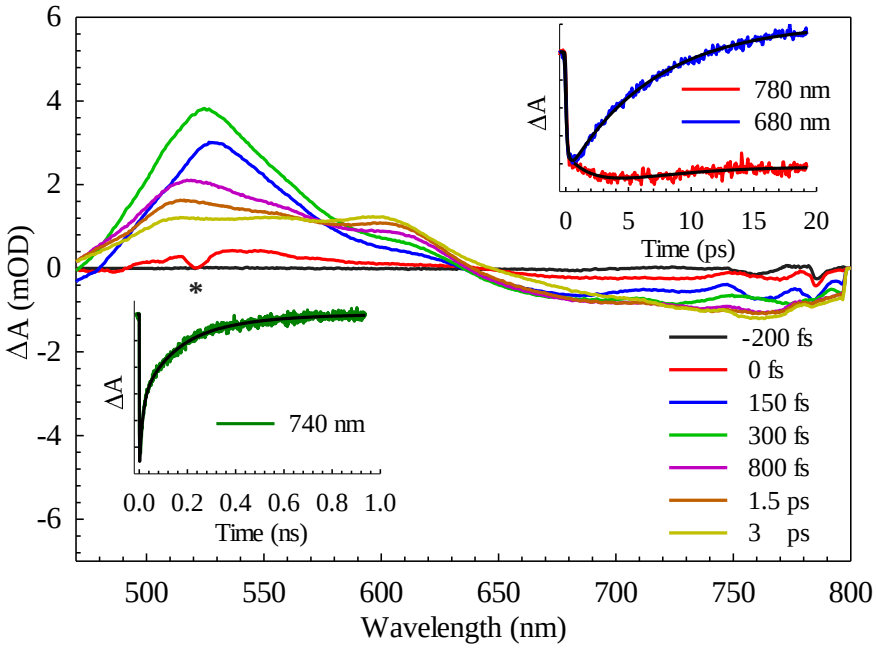

Fig. S6 Transient absorption spectra of 3DHC dissolved in MeOH. The right inset displays solvent dynamics with a rise in the red-side and decay on the blue side of the GSB band. Meanwhile, the left inset exhibits a longer time decay range (refer to Table 2 in the paper for specific time constants). The distorted band at 0 fs delay time (*) illustrates the emergence of Raman scattering due to solvent. IRF = 120 fs, λ_{ex} = 450 nm.

Density functional theory calculations

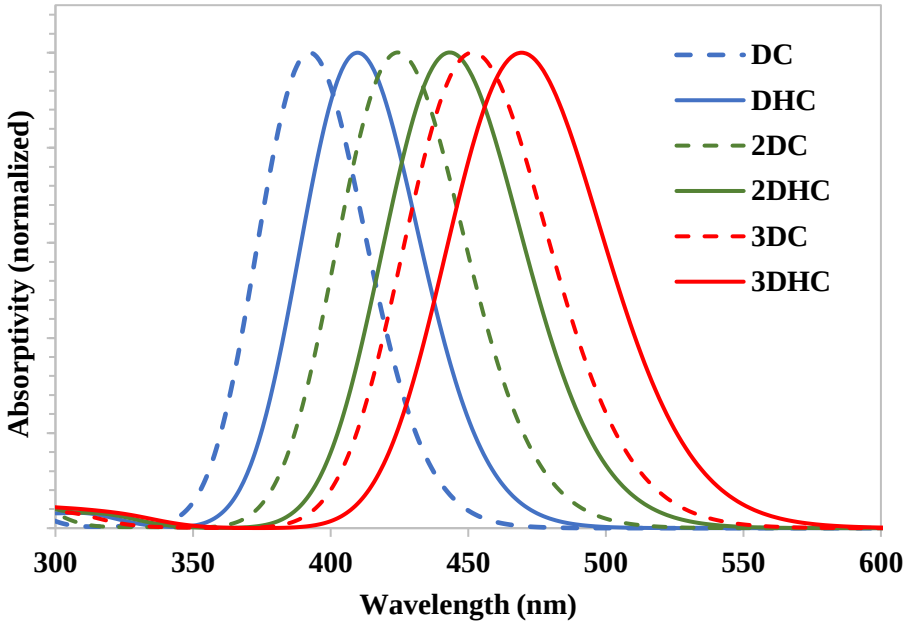

Fig. S7 TD-DFT predicted absorbance derived from the S_0 to S_1 vertical excitation energy. A Gaussian convolution with an arbitrary FWHM of 3000 cm^{-1} has been applied. A small contribution from higher excited states is seen at the shortest wavelengths. Details of the calculation are given in the paper.

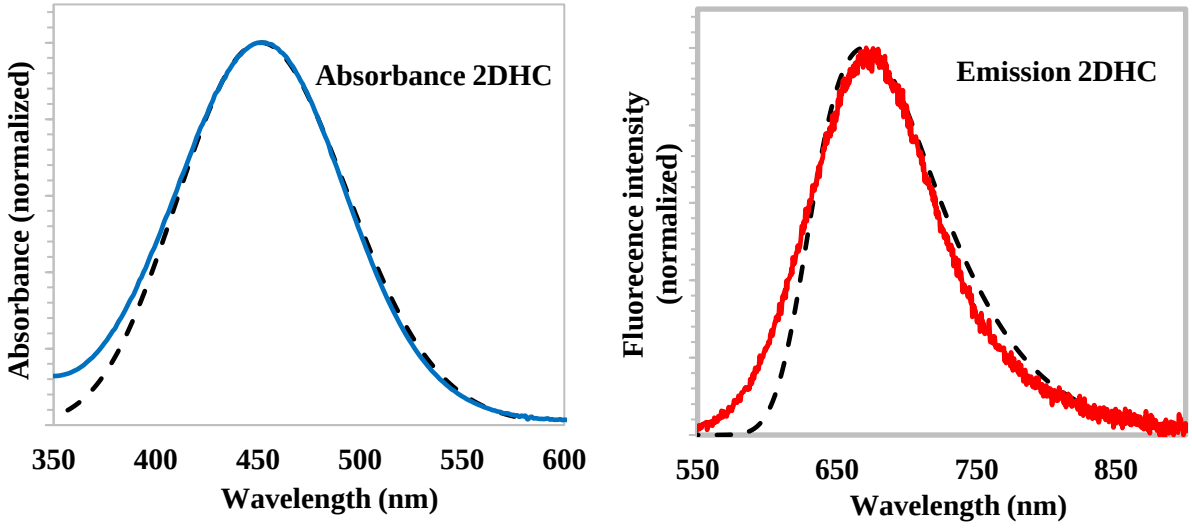

Fig. S8 Calculated vibrational frequencies in the ground and excited states are used to simulate the absorbance and emission band shapes. Shown here for 2DHC as a representative example. To compare with the observed bands (solid colored lines) the predicted spectra have been convoluted with a Gaussian distribution of FWHM 2000 cm^{-1}. The absorbance peak is positioned as calculated, while a red-shift of 130 nm is needed to align the emission peak with the observed band.

Table S2 Selected TD-DFT data. Vertical excitation energies for $S_1 \leftarrow S_0$ at the S_0 optimized geometry are used to estimate λ_{abs}, while those at the S_1 optimized geometry are used for λ_{em}. Oscillator strengths (f) are given for both sets of transitions, and the principle molecular orbital contributions are listed for absorption. The change in dipole moment (μD) is calculated as $\mu_{excited} - \mu_{ground}$.

	λ_{abs} (nm)	f	Orbital contribution	λ_{em} (nm)	f	Δμ (D)
DHC	409	1.43	H → L (89%) {H-3→ L (3%); H → L+1 (3%)}	472	1.56	3.4
2DHC	443	1.87	H → L (88%) {H-1→ L (6%); H → L+1 (4%)}	553	2.07	6.1
3DHC	469	2.29	H → L (84%) {H-1→ L (7%); H → L+1 (5%)}	664	2.56	10.2
DC	392	1.29	H → L (90%) {H-4→ L (2%); H → L+1 (3%)}	456	1.39	2.7
2DC	424	1.76	H → L (88%) {H-1→ L (6%); H → L+1 (4%)}	536	1.94	5.1
3DC	451	2.19	H → L (85%) {H-1→ L (7%); H → L+1 (5%)}	623	2.45	7.70

Table S3 Selected TD-DFT data. Vertical excitation energies (nm) for $S_n \leftarrow S_0$ at the S_0 optimized geometry for the first 10 excited states.

S_n	DHC	2DHC	3DHC	DC	2DC	3DC
S_1	409	443	469	392	424	451
S_2	310	316	324	327	332	334
S_3	304	308	310	280	287	304
S_4	280	288	302	253	273	285
S_5	255	275	286	252	256	270
S_6	248	259	274	245	254	257
S_7	242	250	254	244	250	255
S_8	240	247	250	237	248	250
S_9	233	239	238	230	236	235
S_{10}	225	229	236	218	223	232

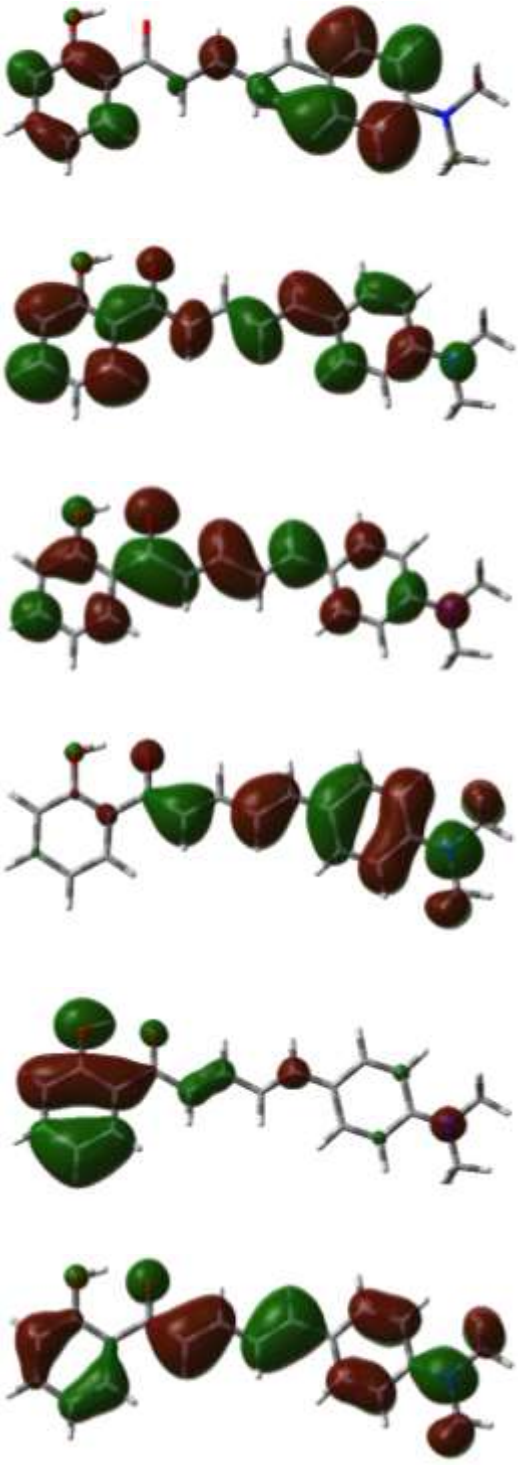

Fig. S9 Frontier molecular orbitals for 2DHC as a representative example. Longest wavelength absorption corresponds to a HOMO to LUMO transition (88%) and moves electron density from the donor to the acceptor portion of the molecule

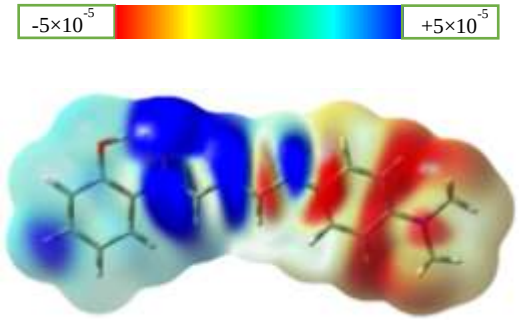

Fig. S10 Electron density difference, $S_1 - S_0$, mapped onto the total S_0 electron density for 2DHC. Areas in blue (positive values) represent regions where the electron density is greater in the excited state than the ground state. The mapping demonstrates the movement of electron density from the donor portion to the acceptor upon excitation.

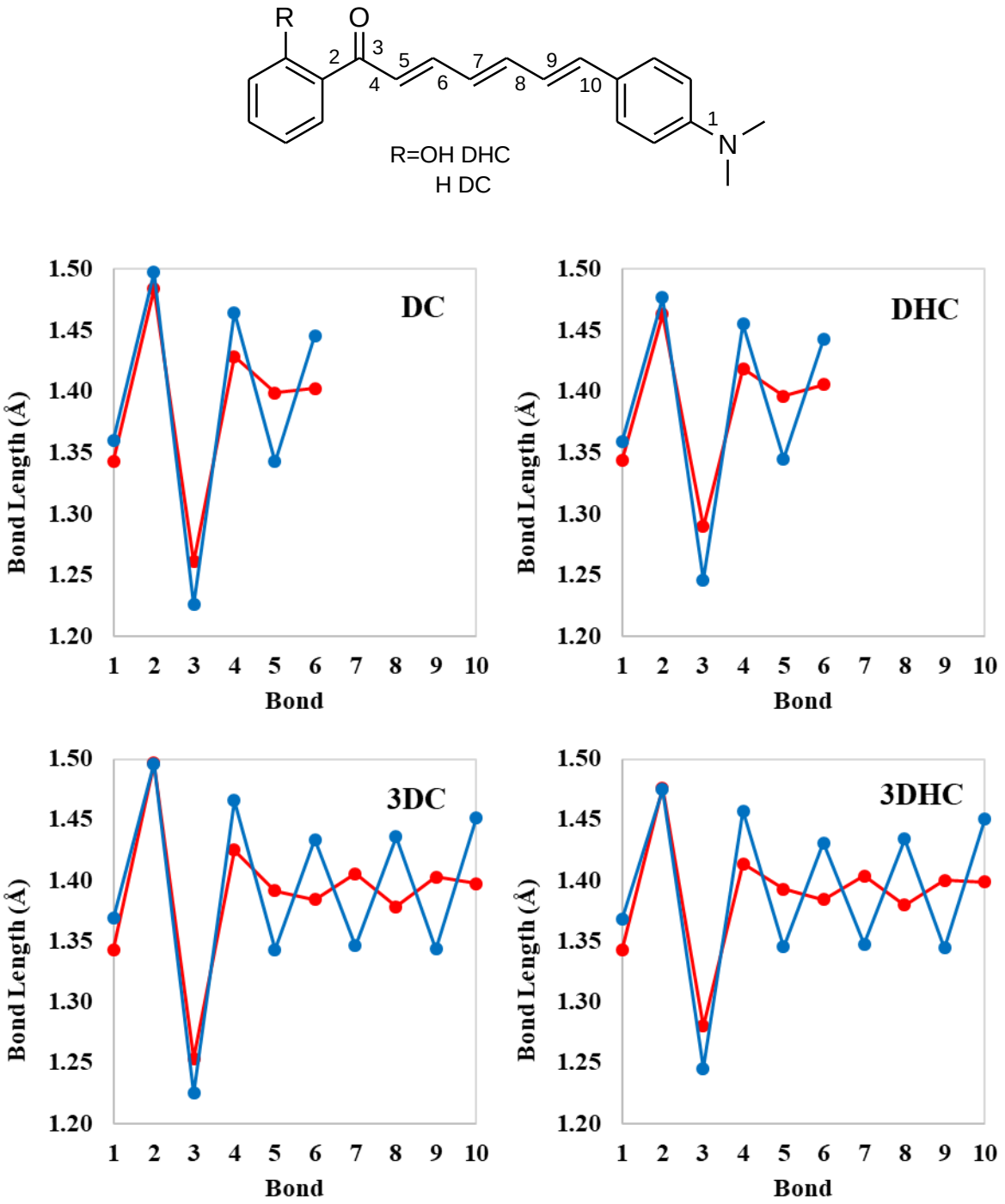

Fig. S11 Selected bond lengths in the S_0 (blue) and S_1 (red) states of the shown molecules. Bonds are numbered as indicated in the top panel. After excitation to the excited state, relaxation results in a lengthening of the C=C double bonds and a shortening of the single bonds. The amine (#1) and carbonyl (#3) bonds are also affected, while bond #2 remains essentially unchanged.

References

1. N.I. Zahid, M.S. Mahmood, B. Subramanian, S.M. Said, O.K. Abou-Zied, New insight into the origin of the red/near-infrared intense fluorescence of a crystalline 2-hydroxychalcone derivative: a comprehensive picture from the excited-state femtosecond dynamics, *Phys. Chem. Lett.* 8 (**2017**), 5603.
2. A.R. Ibrahim, H.N. Lim, O.K. Abou-Zied, N.M. Huang, P. Estrela, A. Pandikumar, Cadmium sulphide nanoparticles decorated with Au quantum dots as ultrasensitive photoelectrochemical sensor for selective detection of copper (II) ions, *J. Phys. Chem. C* 120 (**2016**), 22202.